



Birefringence in Me-CdP₂ photodiodes

I.G.Stamov¹, N.N.Syrbu^{2*}, L.Nemerenco², V.V.Zalamai³

¹T.G.Shevchenko State University of Pridnestrovie, 25 Oktyabrya street 107, 3300 Tiraspol, (REPUBLIC OF MOLDOVA)

²Technical University of Moldova, 168 Stefan cel Mare Avenue, 2004 Chisinau, (REPUBLIC OF MOLDOVA)

³Institute of Applied Physics, Academy of Sciences of Moldova, 5 Academy Street, 2028 Chisinau, (REPUBLIC OF MOLDOVA)

E-mail: sirbunn@yahoo.com

ABSTRACT

In the paper it is researched the spatial dispersion in CdP₂ crystals. The dispersion is positive $n^k \parallel \epsilon > n^k \parallel \gamma$ in the $\lambda > \lambda_0$ region and negative $n^k \parallel \epsilon < n^k \parallel \gamma$ in $\lambda < \lambda_0$ region. CdP₂ crystals are isotropic in case of $\lambda_0 = 896\text{nm}$ and a transmission maximum is observed in case of cross polarizers ($\Delta n = n_o - n_e = 0$). The refractive index $n^k \parallel \epsilon$ is higher in the long wavelength region in reference to λ_0 than the refractive index in case of $n^k \parallel \gamma$ polarization, the dispersion is positive. In the short wavelength part an inverse dependence is observed and the dispersion is negative. Current-voltage characteristics had been researched for Me-CdP₂ diodes at different temperatures, temperature dependencies of “imperfection” coefficient δ for different Schottky barriers. The voltage dependence of capacitance had been studied for Me-CdP₂ photodiodes obtained by electro-chemical deposition of metal and thermo-chemical metal spraying in vacuum. The dependence of diffusion potential Φ_B on the metal work function $\xi_m(C)$ has been revealed. The influence of birefringence and gyration on spectral characteristics of p-n photodiodes and Schottky diodes has been determined. The ability of controlling photodiodes’ characteristics was obtained using the features of gyration in CdP₂ crystals. © 2015 Trade Science Inc. - INDIA

KEYWORDS

Semiconductor compound;
Optical absorption and transmission spectra;
Volt - capacity characteristics;
CdP₂ crystals;
Birefringence;
Photodiodes.

INTRODUCTION

CdP₂ is a wide band semiconductor material of A²B⁵ group, which possesses the anisotropy of optical properties with natural gyrotropy^[1-3]. Polarized spectra are observed in the electronic transitions and vibrational modes, in photoluminescence, photoconductivity, absorption, and reflection^[3-12]. Based on

CdP₂ crystals there were developed devices for quantum electronics and nonlinear optics, which principle of operation is based on gyrotropic and nonlinear polarizability. The values of nonlinear polarization and gyrotropy of cadmium diphosphide are higher than for other crystals, and provides effective stabilization of the radiation field at the same time in space (cross-section) and in time^[13].

Full Paper

Inertialess intensity saturation of the transmitted light through the sample in dependence on the intensity of incident light allows implementing instant feedback on the current radiation field and creating stabilizers of radiation field and laser pulse extenders. Deflectors' advantage is that they can be used in the visible and near-infrared spectrum^[14, 15].

In cadmium diphosphide it was found a linear relationship between the rotating polarization of plane-polarized light and the magnetic field^[16, 17] and the possibility of creating magneto-optical modulators, magneto-sensitive elements to measure the magnetic field, all based on cadmium diphosphide was shown.

Cadmium diphosphide has a high photosensitivity and intense luminescence^[3-5]. The technology of producing *p-n* junctions and surface barrier diodes was elaborated based on CdP₂ crystals^[2, 3, 5-9]. Photoresists built on CdP₂ have a small time constant of relaxation and are suitable for the registration of pulse radiation flows with a duration of $1 \cdot 10^{-9}$ s. Photoelectric emitters and photodiodes^[18-20], electrical switches^[21, 22] and Zener diodes^[23] had been developed based on single CdP₂ crystals. CdP₂ crystals alter the optical activity with temperature, while maintaining the linear dependence of the rotational plane of polarization on the temperature (temperature sensors)^[24].

The properties of birefringence on perfect, high-quality CdP₂ crystals, the CURRENT-VOLTAGE characteristics, capacitance-voltage characteristics, and photovoltaic characteristics of *p-n*-(CdP₂) struc-

tures, *n-p*-(CdP₂), and Me-CdP₂ diodes are studied in this paper. A comparison of the characteristics of device structures obtained by the electrochemical deposition of metal and vacuum thermochemical metal spray was made. The influence of the gyration phenomenon on the characteristics of *p-n* photodiodes and Me-CdP₂ photodiodes was studied.

EXPERIMENTAL METHOD

The process of growing single crystals of cadmium diphosphide from Cd and P precursors occurred in two stages. The cleaning the source of atomic materials and synthesis of CdP₂ chemical compounds was made in the first phase. Synthesis was carried out in quartz ampoules in a high pressure container (≈ 40 atmospheres). Up to 300-500 grams of the substance has been synthesized simultaneously. The synthesized compound was sublimed in a vacuum to obtain single crystals in the second phase. The maximum dimensions of CdP₂ ingots obtained from gas phase reached $15 \times 15 \times 30$ mm. Single crystals had been cleaved perpendicularly to the C axis. Measurements were carried out on single crystals obtained in a form of prisms or plates, which have grown along the C axis, having mirror, non treated surfaces. Schottky diodes, *p-n* junctions, were, also, obtained on cleaved, non polished surface. The absorption spectra were measured at 2 K and 4.2K in a glass cryostat with liquid helium, using the DFS-24 spectrometer with a resolution of $5 \text{ \AA}/\text{mm}$. Optical transmission spectra

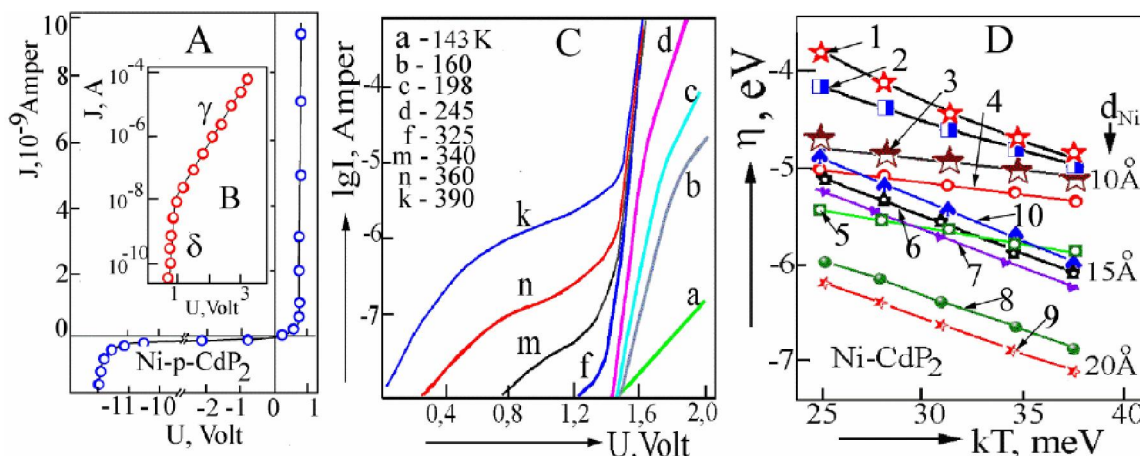


Figure 1 : A, B - Current-voltage characteristics of Ni-CdP₂ diodes; c - photodiode reverse branches at different temperatures; D - temperature dependence of the "imperfection" coefficient δ for $d=10 \text{ \AA}$ (curves 1,2,3), for $d=15 \text{ \AA}$ (curves 4,6,7), for $d=20 \text{ \AA}$ (curves 5,8,9) and curve 10-experiment, for all curves $D_s=(5,10,50) \times 10^{35} \text{ J}^{-1} \text{ m}^{-2}$

were measured using crossed polarizers and the MDR-2 and JASCO-671 spectrometers. Low-temperature measurements were made in a LTS-32C330 Workhorse-type Optical cryostat.

EXPERIMENTAL RESULTS AND DISCUSSIONS

Photodiode manufactured as Ni-CdP₂ structure using the electrochemical coating layer of nickel on the surface of the etched CdP₂ crystal is presented in Figure 1, A. Near-surface region of CdP₂ crystals has depleted phosphorus to a depth of no more than a micron. The p-domain is obtained by the diffusion of Hg or S for a number of structures. Nickel layer electrochemically deposited on the cleaved surface forms a “close” contact with the semiconductor. The volume of the crystal is an n-type conductivity semiconductor with a carrier density of 4.7·10¹⁷cm⁻³ order, due to an excess of phosphorus. The potential barrier height for the diodes obtained by electrochemical deposition is 1.15 eV and 0.3 eV, being higher than in a vacuum deposited diodes^[2, 3]. Potential barrier height was determined from current-voltage and capacitance-voltage characteristics.

The current-voltage characteristics (CVC) of Ni-CdP₂ photodiode are presented in Figure 1, A and Figure 1, B. The current varies in the range (1÷3) × 10¹² Å/cm² in the reverse bias voltage, in case of changing the diode voltage from 0V to 7 V. Thus, the maximum operating current is less than 10¹² Å/cm²[2]. This parameter is comparable to the dark current of photomultipliers. In a direct branch of the CVC two sites (δ and γ) are observed. The current varies dramatically within 10⁻¹²-10⁻⁸Å on the δ section when shifting voltage from 0V up to 0.8 V. The shift increase from 0.8V to 6V changes the CVC slope (section γ)^[2, 3]. This change of forward current with the applied voltage is due to voltage drop across the serial resistances. The availability of γ part in CVC characteristics plays a positive role. It is not necessary to make connections limiting resistors for limiting current in these diodes. This improves the parameters of RC-circuit. The measurement of small signals can be done using Ni-CdP₂ diode without applying bias voltage. The reduction of the bias de-

creases the value of the reverse currents of the diodes. Extrapolating the line branch of the CVC down to the bias voltage, which approaches zero, it was estimated the limit value of reverse currents ≈ 10¹⁷Å/cm². It is possible to implement such a magnitude of reverse currents if providing minimum surface leakage currents. Thus, one can expect reverse currents of 10-15 A/cm² values if implementing constructively the diode with a guard ring.

The study of reverse CVC branches of Ni-CdP₂ diodes (Figure 1C, 2C) shows that the breakdown occurs at a 5.3V voltage and T ≤ 340K. The CVC is linear down to the breakdown voltage for barriers with Ni, Cu, and Pt metals. The linearity is observed up to 400 K temperature range for In-CdP₂ barriers. The CVC dependence is determined by the thermo-electron field mechanism for Sn-CdP₂ contacts.

The nature of the breakdown is a tunnel one, which is confirmed by a weak decrease in the breakdown voltage (breakdown) with temperature increasing, and by the CVC characteristics' linearity at the site of the breakdown, in the coordinates:

$$\log \left[\frac{J}{(\varphi_B - \mu_F - U)} \right] = f(\varphi_B - \mu_B - U)^2 \quad (1)$$

The dependence of the breakdown voltage on the temperature can be empirically expressed by the following relationship:

$$U = U_{bd}(T_0) - \beta(T_0 - T) \quad (2)$$

The effective mass of charge carriers is estimated from the slope of the CURRENT-VOLTAGE at this part:

$$m^* = 4.118 \cdot 10^{-27} \frac{N}{\epsilon_s \varphi_B^3} \frac{\Delta \lg J / (\varphi_B - gU)}{\Delta (\sqrt{\varphi_B - U})} \quad (3)$$

The effective mass was (0.012-0.027) m₀ in all structures. Similar values were obtained from the temperature dependence of the current J₀.

The temperature dependence of the direct branch of CVC of Ni-CdP₂ photodiodes is shown in Figure 2, A. In regarded Schottky diodes the dependence of the current on the voltage, at voltage values of 0.05 < U < 0.28 is described by the relation:

$$J = J_0 \exp \frac{qU}{\eta kT} \quad (4)$$

Where U – direct voltage, η – “imperfection” index, and J₀ – the current for the thermionic emission

Full Paper

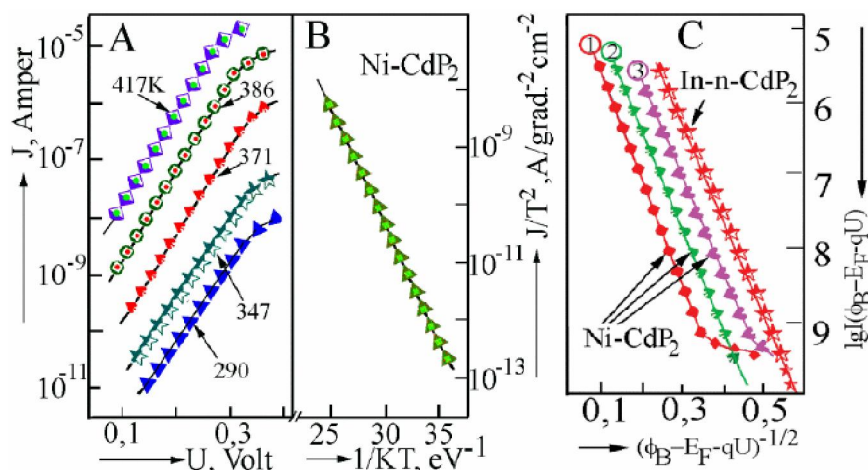


Figure 2 : Temperature dependence of the direct branch of CVC (A) and of the photocurrent (B) of Ni-CdP₂ diodes and C – CVC at the site of Schottky Ni-CdP₂ (1-3) and In-n-CdP₂ (4) breakdown

TABLE 1 : Schottky diodes' parameters obtained by electrochemical deposition of metals on the cleaved surface of CdP₂ crystals

Metal	ϕ_B , eV (Current-voltage)	ϕ_B , eV (volt-capacity characteristic)	N, M ⁻³	η (300K)
In	0.68±0.02	0.66±0.01	3.6×10 ²³	1.08±0.02
Cu		0.85±0.01	2×10 ²³	1.07±0.02
Ni	0.90±0.02	0.90±0.01	2×10 ²³	1.03±0.01
Ni		0.83±0.01	7×10 ²²	
Ni		0.85±0.01	6×10 ²²	
Pt		1.20±0.02	5×10 ²¹	1.1±0.02

is given by:

$$J_0 = A^* T^2 \exp\left(\frac{\phi}{kT}\right)^{-1}, \quad A^* = \frac{qm^* k^2}{2\pi^2 \hbar^3} \quad (5)$$

Where m^* - effective mass of charge carriers. There is a good correlation between the theoretically calculated dependence and the experimental data. The dependence $J_0 = f(T)$ is shown in Figure 5, B. The Ni-CdP₂ barrier height determined from the experiment was 0.9 ± 0.01 eV, the effective Richardson constant $A^*=2$, which corresponds to the effective mass of electrons $0.016m_0$.

The “imperfection” index varies with temperature at high temperatures for the Ni, Cr, Pt-GaAs Schottky barriers^[2], which is explained by the imperfection of Me-p-p contact, by the presence of an intermediate layer thickness d and the density of surface states D_s ^[2, 3, 6-8].

According to the data obtained for Ni-CdP₂, the current that flows through the junction depends on the voltage:

$$J \sim \exp\left\{\left[\frac{q}{\eta_1 kT} + \alpha(\eta_2 - 1)\right] \frac{U}{\eta_2}\right\} = \exp\frac{qU}{\eta kT} \quad (6)$$

Where η_1 – “imperfection” coefficient, $\eta_2 = 1 + \frac{U_2}{U_1}$, η_2 – characterizes the distribution of stresses between the dielectric gap and Schottky barrier spatial charge region,

$$\eta_2 = 1 + \frac{dq^2 D_s}{\epsilon_i \epsilon_0} \quad (7)$$

Where ϵ_i - dielectric constant of the interlayer,

$$\alpha = \frac{d}{h} \sqrt{\frac{m^*}{2V_*}}, \quad \text{and} \quad V_* = \frac{q\hbar}{2} \left[\frac{N}{m^* \epsilon \epsilon_0} \right], \quad \alpha -$$

characterizes the probability of tunneling charge carriers through the intermediate layer. Figure 1, D shows the dependence of $\eta=f(T)$, calculated according to the expression (7) with $\epsilon_i=10$, $m^*=0,1m_0$. η for Metal-CdP₂ contact is presented for comparison (curve 10). A similar dependence of

TABLE 2 : The parameters of the Me - CdP₂ Schottky barriers obtained by metal spray in vacuum on the cleaved surface of CdP₂ crystals ($n=2 \times 10^{22}$, m⁻³)

Metal	Ga	In	Pt	Sb	Ag	Cu	Te	Au
ξ , eV	2.75	3.8	4.0	4.8	4.3	4.4	4.7	4.8
ϕ_B , eV	0.37	0.81	0.65	0.94	1.03	1.15	1.2	1.17

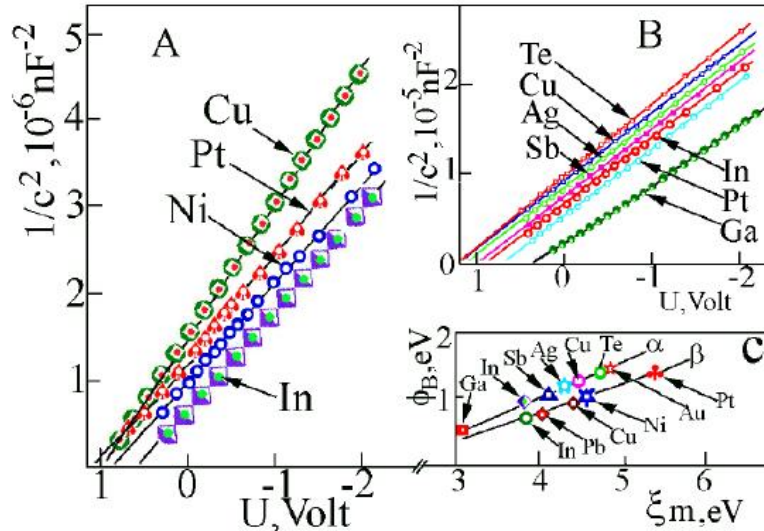


Figure 3 : Volt - capacity characteristics of Ni-CdP₂ obtained by electrochemical deposition of metal (A), volt - capacity characteristics of Me-CdP₂ photodiodes obtained by thermo-chemical metal spray in vacuum (B), dependence of the diffusion potential Φ_B on the work function of the metal ξ_m (C)

the direct branch of the CVC in this voltage range is observed in the metal-In, Cu, Pt barriers^[2, 6]. The “imperfection” index consisted 1.05 – 1.33 for different samples at T=300K. The Schottky diodes’ parameters are presented in TABLE 1 and 2.

Figure 3 shows the typical dependence of the capacitance on the voltage of Me-CdP₂ diodes obtained by the electrochemical deposition of metals. The height of the barrier: $\phi_B = \phi_{III} + \mu_F - KT - \Delta\phi$, where μ_F – energy value, measured from the bottom of the conduction band E_c to the Fermi level E_F , KT – additive in the barrier height due to the influence of mobile carriers, $\Delta\phi$ – lowering of the barrier height due to the forces of mirror image are determined from these characteristics. Figure 3, C shows the values of barrier heights obtained by electro-deposition (curve- α) and by thermal spraying in vacuum (curve- β). It is evident that the value of the barrier heights obtained by thermal spray is higher than that for the diodes obtained by chemical deposition^[2, 6]. The values of the Me-CdP₂ barrier heights is described by a linear dependence $\phi_B = A\xi_m + B$, on the work function of the metal, where $A=0.35$, $B=-0.7$

eV (Figure 3, curve β) and $A=0.4$, $B=0.8$ eV (Figure 3, curve α). This relation defines the density of surface states D_s , averaged over the band gap, which is equal 2×10^{13} eV⁻¹m⁻², and is close to the value obtained from the temperature dependence on the “imperfection” coefficient.

The values of the potential barrier are estimated by us from the photovoltaic characteristics (Figure 4). The photocurrent is conditioned by the emission from the metal into the semiconductor in the photon energy region $E < E_g$, in the absence of impurity absorption. According to the theory the frequency dependence of the photoemission current is determined by the parabolic law: $J_{ph} = 0$ for $E < E_g$ and $J_{ph} = A_0 (E - E_g)^2 / 2K^2$ for $E > E_g$ ^[2, 6]. The potential barrier height of Me-semiconductor structures is determined from the dependence $J_{ph}^{1/2} = f(E)$. The dependence of photocurrent on the energy for Au-, In-, Cu-, Ni-CdP₂ barriers is presented in Figure 4. It is evident that the barrier height depends on the metal and on the orientation of the crystal surface. As the voltage increases the displacement value ϕ_B decreases.

The Fauler emission appears in the energy re-

Full Paper

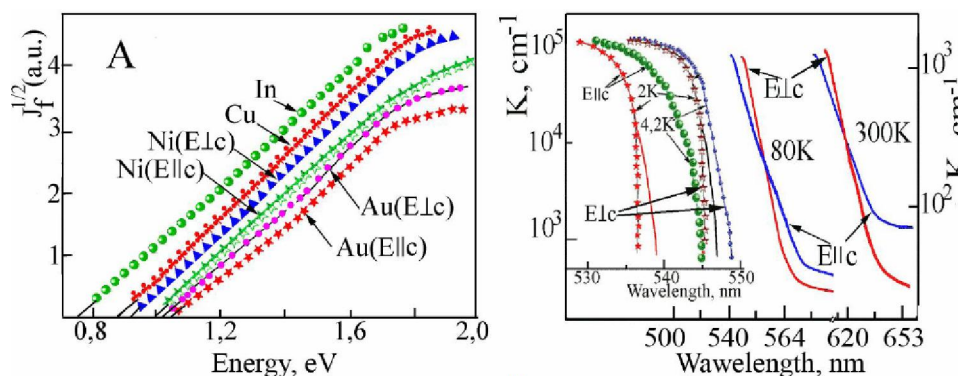


Figure 4 : A – Spectral dependence of photocurrent $J_{ph}^{1/2}$ for Schottky diodes for the $E < E_g$ region. B – Anisotropy of boundary absorption of CdP₂ crystals at 300K, 77K, 4.2K and 2K temperatures

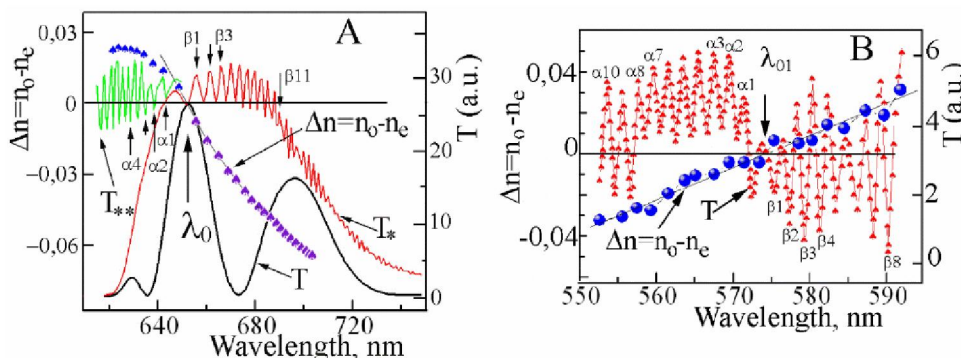


Figure 5 : A – Transmittance spectra (T) of CdP₂ crystals with 0.47mm thickness, interference of transmittance spectra (T_e) of crystals with 0.29mm thickness and 0.187mm thickness (T_{**}) placed into crossed polarizers and the spectral dependence $\Delta n = n_o - n_e$ determined from interference spectra; B – interference of transmittance spectra T of crystals with 1.7 μ m thickness and the spectral dependence $\Delta n = n_o - n_e$ in λ_{01} vicinity

gion 0.7-1.1eV. At zero bias the barrier for CdP₂ crystals and In, Ag, Cu, Te, Au metals on the surface (100) are respectively 0.78, 0.89, 0.93, 0.97, 1.03eV. The obtained values of the barrier heights using this method are consistent with the values of the barrier heights determined from electrical measurements. This confirms the thermoionic – field mechanism of current transport in metal-CdP₂ contact. The dependence of the photocurrent $J_{ph}^{1/2} = f(E)$ in the plane (100) for the E \parallel c and E \perp c polarizations is almost the same, but the magnitude of the potential barrier height for the E \perp c polarization is less than that for E \parallel c polarization. This is consistent with anisotropy of the CdP₂ crystal absorption presented in Figure 4. The temperature influence on the photocurrent for Au-CdP₂ (100) barriers was studied in^[26, 23]. There is a slight reduction of the entry associated with the displacement of the Fermi level and the change of the band gap with temperature increase.

The edge absorption of CdP₂ single crystals at room temperature begins with a gentle rise of the

absorption coefficient for both polarizations (E \parallel c and E \perp c). Lowering the temperature leads to a shift of the absorption boundary to shorter wavelengths. Several features of E \parallel c and E \perp c polarizations, which are characteristic for indirect transitions in the exciton band with the emission of phonons, exhibit in spectra at low temperatures, in the region of low absorption coefficients. The energy position of these features conditioned by the phonon emission is almost identical in both polarizations. The threshold value of the zero-phonon transition towards the indirect exciton zone is the same and equals 2.1547eV in case of E \parallel c and E \perp c polarizations within the experimental error (0.0005 eV). However, the absorption value in the $E < E_g$ region for both polarizations E \parallel c and E \perp c vary and intersect at 300 and 77 K, Figure 4. The absorption in the E \parallel c polarization is higher than for E \perp c in the energy region \sim 1.9eV at 300 K. In the $E > 2$ eV region the absorption coefficient is reversed, i.e. the absorption is higher at E \perp c polarization than at E \parallel c polarization. The same de-

pendence is present at 77K and at helium temperatures.

Polarized boundary absorption is observed in the region $E > 2.23$ eV at 2K and 4.2K (Figure 4). The absorption boundary is shifted to lower energies compared to the $E \parallel c$ for $E \perp c$ polarization. The sharp increase of the absorption coefficient in this region is conditioned by the direct allowed transitions. The calculated values of the absorption coefficient are correlating with the experimental data by the following parameters: $E_{gx} = 2.2727$ eV and $A = 3.04 \cdot 10^4$ eV^{1/2}/cm at $E \perp c$ polarization and 2K temperature value, and $E_{gx} = 2.3078$ eV and $A = 2.8 \cdot 10^4$ eV^{1/2}/cm for $E \parallel c$ polarization and 2K temperature value, where:

$$A = \frac{2e^2(2m^*)^{3/2}}{m_0^2 c \hbar^2 n} |P_{cv}|^2 \quad (8)$$

It is clear from these results that the absorption curves of direct allowed transitions at 2K for the $E \parallel c$ and $E \perp c$ polarizations are shifted to 35.1 meV, i.e. the direct transitions occur from minimum two valence bands. These transitions are allowed by the selection rules for different polarizations. Temperature increase from 2 to 4.2K leads to a shift of the absorption curves to longer wavelengths. The temperature coefficient of the offset energy intervals $\Delta E / \Delta T$ are ranged by the direct allowed transitions with temperature change from 2 to 4.2K and equals 10.6 meV/K at the $E \parallel c$ polarization and 3.2 meV/K at $E \perp c$ polarization. Different rates of temperature shift of the absorption boundary for the $E \parallel c$ and $E \perp c$ polarizations indicate that direct transitions occur in two areas V_1 and V_2 .

Figure 5 shows the transmission spectra (T) of CdP₂ crystals with 470 μm thickness, the interference of the transmission spectra of crystals with 290 μm thickness (T_{*}) and 187 μm thickness (T_{**}) placed between crossed polarizers and the spectral dependence $\Delta n = n_o - n_e$ determined from interference spectra. Main peak λ_0 and lateral satellites are observed in the spectra of crystals with 470 μm thickness. Pronounced interference of transmission spectra (T_{*}) adjacent to the wavelength λ_0 is observed in crystals of 290 μm thickness, in $\lambda > \lambda_0$ region. These spectra are due to the interference of ordinary (n_o) and extraordinary (n_e)

lightwaves. The spectral dependence $\Delta n = n_o - n_e$, which is negative, is determined from these spectra. A feature of these spectra is that the distance between the peaks ($\beta_1, \beta_2, \beta_3, \dots$) increases with wavelength decrease. This means that $\Delta n = n_o - n_e$ decreases as the light wavelength decreases (Figure 5, curve $\Delta n = n_o - n_e$). The distance between the peaks of the interference spectra decreases while moving to shorter wavelengths due to higher refractive index and the absence of an isotropic wavelength. Interference spectra and ($\alpha_1, \alpha_2, \alpha_3, \alpha_4$) maxima, which are gathering while decreasing the wavelength, are detected in the wavelength region $\lambda < \lambda_0$, in transmission spectra (T_{**}) of crystals with 187 μm thickness. The difference $\Delta n = n_o - n_e$, which has a positive value is determined from these data. In crystals with 1.7 μm thickness the transmittance is much lower (Figure 5, B). The interference of light waves in the vicinity of the wavelength λ_{01} (574 nm), from which is determined the value $\Delta n = n_o - n_e$, is revealed on these crystals in case of crossed polarizers. With wavelength increase the value $\Delta n = n_o - n_e$ increases from negative -0.04 to 0.04 values, crossing the zero axis at λ_{01} (574 nm) wavelength. The values of the refractive indices n_o and n_e overlap at these wavelength values (Figure 5, B). The intersection of boundary absorption curves occur at these wavelengths and 300K, Figure 4, B. This is due to the fact that the direct transitions occur at lower energies for $E \perp c$ polarization than for the $E \parallel c$ polarization. This is done both at room temperature and at low temperatures. The spectral characteristic of the refractive indices' difference $\Delta n = n_o - n_e$ determined by the Kramers-Kronig method and from the interference, are in complete agreement, the both curves have a zero value at a wavelength of 654 nm and 574 nm, Figure 5, A and Figure 5, B.

A series of maxima and minima are revealed at 10K in the transmission spectra T of CdP₂ crystals positioned between crossed polarizers at $k \parallel c$ (k – lightwave vector, c – crystal axis), which bifurcate at 7-10° change between the axis and the lightwave vector k (curve-T*), Figure 6. The difference value of the refractive index at 10K ($\Delta n = n^y - n^x$) is calculated from the interference spectra, where n^y - refractive index at $E \parallel y$ polarization and n^x - refractive index at $E \parallel x$ polarization, Figure 6. The difference of the refractive index

Full Paper

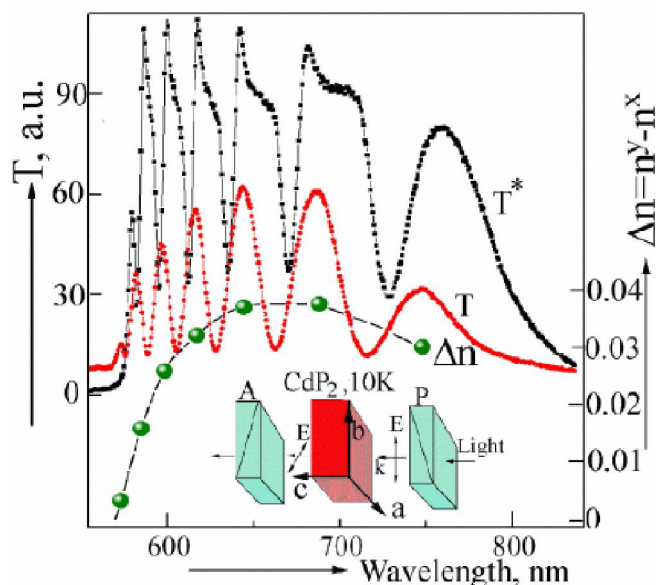


Figure 6 : Spectral dependence of transmittance of CdP₂ crystals placed inside crossed polarizers at $k \parallel c$ (k – lightwave vector, c – crystal's axis) and T^* – at incident angle of $7-10^\circ$ between the axis and the lightwave vector k and calculated values $\Delta n = n^y - n^x$ (n^y – refractive index at $E \parallel y$ polarization and n^x – refractive index at $E \parallel x$ polarization)

reaches, almost, the zero value at 550.7nm wavelength. This wavelength corresponds to λ_{01} , which is detected at 300 K and 574nm wavelength value.

Figure 7 shows the spectral distribution of photo response J_{ph} in non polarized light of ITO-n-p-CdP₂-Au diodes' and the photodiode's structure design. Photodiodes represented n-p- and p-n-junctions based on CdP₂ crystals. These transitions were obtained by doping the original crystal using the diffusion in a closed volume. The phosphorus vapor pressure in a closed volume must be $\sim 3.5-2 \cdot 10^{-1}$ atmospheres in order to save the parameters of the initial composition. In such a mode, controlled by the reference samples, the diffusion of atoms of mercury and sulfur was carried out. The concentration of charge carriers in the samples with $n=4 \cdot 10^{16}$ changed up to $n=6 \cdot 10^{15} \text{cm}^{-3}$, as a result of the mercury diffusion. In crystals with a concentration of $n \sim 10^{16} \text{cm}^{-3}$ the conductivity was changing from n-type to p-type ($p=1.2 \cdot 10^{16} \text{cm}^{-3}$). In the paper it was assumed that the diffusion process is filling cadmium vacancies with mercury atoms. This is likely because the homeopolar radiuses of cadmium and mercury atoms are almost identical, and differ only by 0.03Å. The spectra of photo-

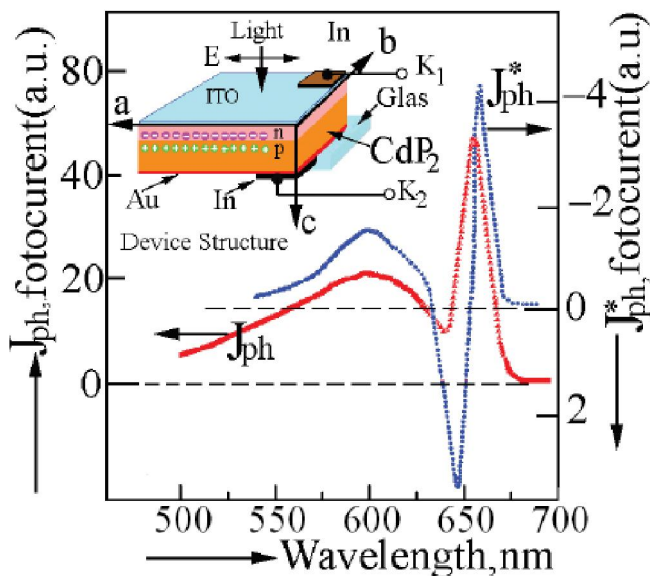


Figure 7 : Spectral distribution of J_{ph} photo response in case of unpolarized light; J_{ph}^* at EQ%a polarization of ITO-n-p-CdP₂-Au diodes and photodiode structure design

electric effect of the structures shown in Figure 7 has an intense maximum of the photo response at 654 nm wavelength in case of unpolarized light and a flat maximum at 570-600 nm (curve J_{ph} , Figure 7). These maxima are corresponding to isotropic wavelengths λ_0 and λ_{01} in CdP₂ crystals. The curve J_{ph}^* is also contain two maxima at almost the same wavelength in $E \parallel a$ polarization, but the negative photoresponse is more than that in the case for J_{ph} .

The presence of high photosensitivity in case of isotropic wavelength λ_0 means that at this wavelength is the most effective interaction of modes in the crystal. Interaction of modes occurs at λ_{01} wavelength, but much weaker. Energy exchange between orthogonally polarized waves occurs in the neighborhood of isotropic point (λ_0) of the crystal. In order to implement the transfer of energy from one orthogonally polarized mode to another, the following conditions are necessary: 1) phase matching; 2) the presence of a coupling element. The first condition is satisfied in anisotropic crystals with an isotropic point, such as CdP₂ crystal.

The interaction between the modes is described by nonzero off-diagonal matrix elements of the dielectric tensor.

$$\frac{\partial^2}{\partial \mathbf{X}^2} \begin{pmatrix} \mathbf{E}_y \\ \mathbf{E}_z \end{pmatrix} = \frac{\omega^2}{C^2} \begin{pmatrix} \epsilon_{yy} & \epsilon_{yz} \\ \epsilon_{yz} & \epsilon_{zz} \end{pmatrix} \begin{pmatrix} \mathbf{E}_y \\ \mathbf{E}_z \end{pmatrix}. \quad (9)$$

In the absence of $\varepsilon_{yx}=0$ interaction the equation (9) has solutions that are characterized by the values of $K_o=(2\pi n_o/\lambda)$ and $K_e=(2\pi n_e/\lambda)$, where K_o and K_e are the wave vector value of the ordinary and extraordinary waves, respectively.

$$n_o^2 = \varepsilon_{yy}, \quad n_e^2 = \varepsilon_{zz}. \quad (10)$$

In case, when $\varepsilon_{yz} \neq 0$, the solutions of equation (9) lead to the following results:

$$K_+ = 2\pi n_+ / \lambda, \quad K_- = 2\pi n_- / \lambda, \quad (11)$$

while:

$$n^+ - n^- = [1 + Y^2(\lambda)]^{1/2} \varepsilon_{yz} / n, \quad (12)$$

where $n = (n_e + n_o) / 2$ is the average refractive index;

$$Y(\lambda) = n(n_e - n_o) / \varepsilon_{yz} = (n_e^2 - n_o^2) / 2\varepsilon_{yz}. \quad (13)$$

The value of Y is experiencing dramatic change when passing through an isotropic wavelength λ_o . If $\varepsilon_{yz} = 10^{-6}$, then Y ranges from 0 to 10^3 , where $\Delta n = n_e - n_o$ changes from 0 to 10^{-3} . Far from λ_o , the Y value is high enough, but varies slightly with λ change. In this area, it appears that $n^+ - n^- = n_e - n_o$. Thus, the ordinary and extraordinary modes' conception lose their value and gain a real sense outside this interval in the neighborhood of λ_o limited by the spectral range of sharp change of Y parameter. The exchange of energy between the modes at λ_o is determined by the connection element ε_{yz} between modes, which is responsible for the high photosensitivity of the studied diodes. The fraction of energy that is transferred out of the mode, polarized along the Y axis into the mode polarized along the Z axis, after traveling a distance X in the crystal, is given by the expression (14):

$$J_T(x, \lambda) = [J_y(x) J_z(x)]^{0.5} |\beta|^2 \frac{\sin^2 \left[\left(|\beta|^2 + \left(\frac{\Delta K}{2} \right)^2 \right)^{0.5} X \right]}{|\beta|^2 + \left(\frac{\Delta K}{2} \right)^2}. \quad (14)$$

In formula (14), $J_y(x)$ is the intensity of modes polarized along the Y axis, after passing through the crystal the X distance in the absence of modes interaction; $J_z(x)$ - the same for the mode, polarized along the Z axis, β - the interaction parameter, proportional to ε_{zz} ,

$$B = \pi \varepsilon_{yz} / n \lambda, \quad \Delta K = \kappa_e - \kappa_o = 2\pi(n_e - n_o) / \lambda. \quad (15)$$

The absorption is low in the transparency re-

gion of the crystal. The derivate of modes' intensity polarized along the Y and Z axis, equals the radiation intensity incident to the crystal J_o , i.e. $J_y(x) J_z(x) = J_o^2$. In the isotropic point of the crystal, where $\Delta k = 0$, the following condition is assured:

$$J_T(x, \lambda_o) = J_o \sin^2(|\beta|x). \quad (16)$$

The appearance of non-diagonal element ε_{zz} of the dielectric transparency tensor (the nature of linkage element) is due to spatial dispersion. The tensor of the dielectric constant of the crystal $\varepsilon(\omega, k)$ depends on the frequency ω and the wave vector K . The following condition is assured for the $\varepsilon_{ij}(\omega, k)$ component of the dielectric constant:

$$\varepsilon_{ij}(\omega, k) = \varepsilon_{ij}(\omega) + i\gamma_{ijl}(\omega) \kappa_l + \alpha_{ijlm}(\omega) \kappa_l \kappa_m + \dots \quad (17)$$

i.e. the expansion of $\varepsilon_{ij}(\omega, k)$ in powers of k is provided if $\varepsilon_{ij}(\omega, k \rightarrow 0) = \varepsilon_{ij}(\omega)$.

In (17) $\gamma_{ijl}(\omega)$ and $\alpha_{ijlm}(\omega)$ are the tensors of the third and fourth rank, that describe the spatial dispersion of the first- and second-order, respectively. Effects under consideration occur to the spatial dispersion of the first order (gyrotropy), and are described by values of α/λ order, where α - lattice constant.

The photosensitivity of ITO-n-p-CdP₂-Au diodes (curve J_{ph}^* , Figure 7) contains two peaks at $E||$ a polarization. Spectral response of photosensitivity has an intense peak at 656nm wavelength, and, crosses the wavelength 654nm, while decreasing the wavelength and has negative electromotive force (EMF) value at 652nm wavelength.

This characterization of photosensitivity is conditioned by the competing photo-voltage mechanisms, which appears in the ITO-n-p-CdP₂-Au structure. In the long-wavelength range of isotropic point (λ_o) the lightwaves penetrate deeper and create photo-EMF in the spatial charge carriers region of the Au-CdP₂ Schottky diode, which has a positive value (J_{ph}^* curve, Figure 7). With decreasing wavelength the absorption coefficient increases, while there is a gyration - the polarization plane rotation of lightwaves near the isotropic wavelength. This leads to the excitation of the charge carriers in the spatial charge region of n-p-CdP₂, which photo-EMF is negative.

Figure 8, A shows the transmission spectra T_a at $E||a$ polarization, T_b at $E||B$ polarization in CdP₂ crys-

Full Paper

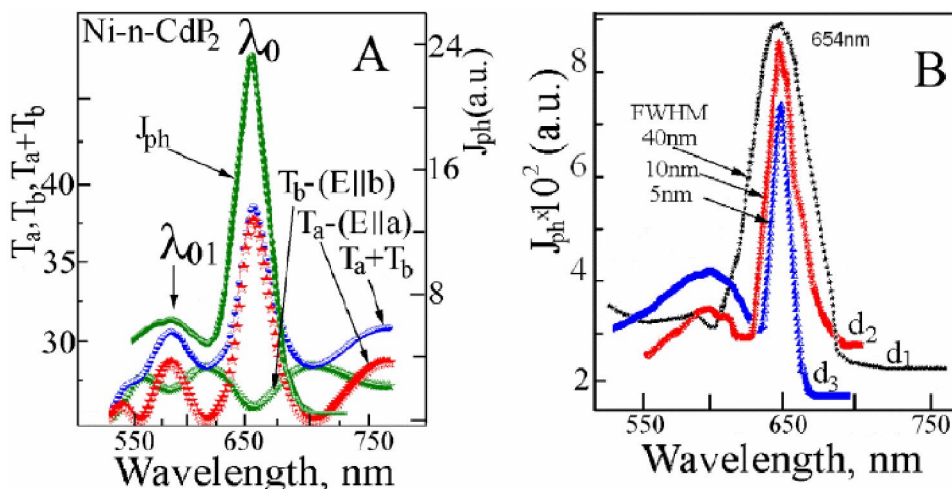


Figure 8 : A – Transmittance spectra of CdP₂ crystals with thickness 1.01mm, T_a at E||a polarization, T_b at E||B polarization and the sum of transmittance coefficients T_a + T_b and the photosensitivity J_{ph} of Ni-n-CdP₂ diode in case of unpolarized light; B – The spectral distribution of the photosensitivity near the isotropic point (λ_0) of the diodes obtained on crystals with $d_1=1.01$ mm, $d_2=0.630$ mm, and $d_3=0.41$ mm thicknesses.

tals with $d=1.01$ mm thickness and the total transmittance T_a+T_b . The transmittance spectra are considered in near isotropic wavelength (λ_0). The peaks in the spectra of T_a at E||a polarization correspond to the minima T_b at E||B polarization in this region. The transmission spectra curve T_a+T_b almost matches the transmittance spectra of crystals of this thickness placed between crossed polarizers. Intense maximum of transmittance spectra T_a+T_b coincides with the λ_0 wavelength maximum of J_{ph} photosensitivity of Ni-n-CdP₂ diode at unpolarized light. The spectral distribution of the photosensitivity near the isotropic point (λ_0) of the diodes obtained on crystals with $d_1=1010$ nm, $d_2=630$ nm and $d_3=410$ nm thicknesses (Figure 10, B) shows the change of the halfwidth of FWHM bandwidth photosensitivity J_{ph} of the diodes with a peak at λ_0 wavelength. The transmittance coefficient T is described by the expression $T=\sin^2(\rho d)$, where ρ is the magnitude of the specific rotation at λ_0 wavelength and at the same time the interaction constant. Transmission coefficient can be expressed as:

$$T = \frac{\sin^2(\pi/\lambda) \left[(\delta n^2 + \Delta n^2)^{0.5} d \right]}{1 + (\Delta n / \delta n)^2}, \quad (18)$$

Where $\Delta n = n_e - n_o$ – crystal's linear birefringence; $\delta n = \lambda \rho / \pi$ is the circular birefringence; d – thickness of the crystal element. It follows from this expression that the optimum thickness of the crystal, corresponding to the maximum bandwidth is $d = \pi / 2\rho_0$, where $\rho_0 = \rho(\lambda_0)$.

Consequently, one can determine under what thicknesses, the maximum bandwidth with the narrowest band can be observed, considering the data gyrotropy. On the basis of gyrotropic crystals such as CdP₂, which have a narrow bandwidth, while placed between crossed polarizers, one can get narrow band sensitivity photodiodes. Figure 9 shows the structure of the two paired photodiodes obtained on the surface layer, connected by the ITO layer, while the C axis of layer 1 is perpendicular to C axis of layer 2, Figure 9. In the lower part of the figure it is shown the transmittance spectra T_a of CdP₂ crystals at E||a polarization and T_b at E||B polarization. The spectral dependence of photosensitivity J_{ph} is measured at E||a polarization of layer 1, and includes a central peak at λ_0 wavelength (654nm) and two side maxima from the short and long wavelength region. The spectral response has, almost, the same character at polarization change of on E||c of the layer 1, but EMF has the opposite sign. This characteristic, along with its peaks, is like in the case of light transmittance spectra along the C axis of the crystal, where there is a rotation of the polarization plane. The curve of the transmittance T spectral dependence of CdP₂ crystals placed between crossed polarizers are shown for comparison, i.e. when the light propagates along the C axis. The gyrotropy property and, naturally, the absorption (transmittance) coefficient and their difference at E||c and E⊥c affect partially

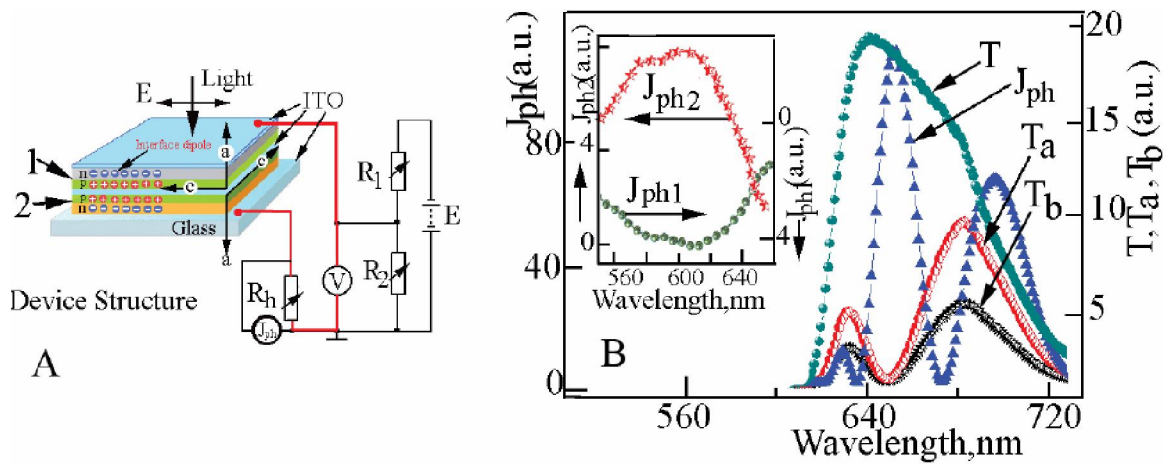


Figure 9 : A – construction of two paired photodiodes obtained on the surface and connected by the ITO layer (C-axis of layer 1 is perpendicular to C axis of layer 2); B – transmittance spectra of CdP₂ crystals at E||a polarization, T_b at E||B polarization, T – transmittance between crossed polarizers and the photo response J_{ph} of the coupled photodiode at unpolarized light

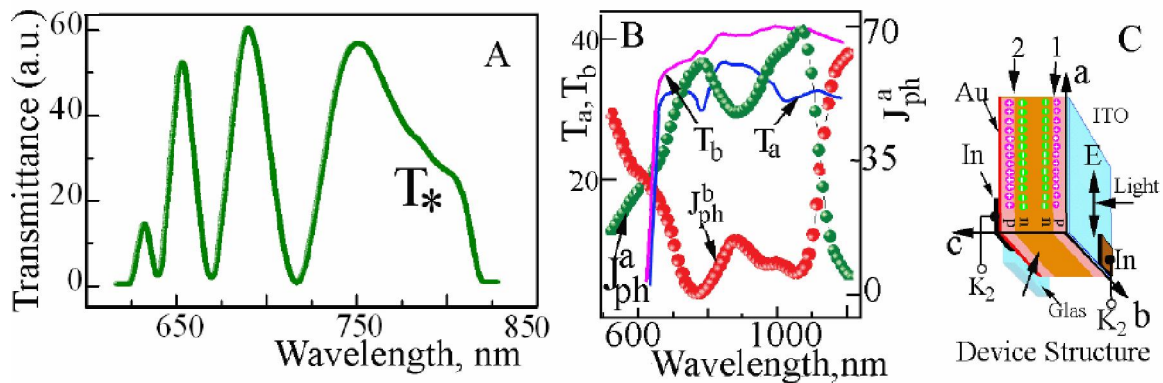


Figure 10 : A – Transmittance spectra T* of CdP₂ crystals doped with sulfur placed between crossed polarizers; B – the photosensitivity of J_{ph}^a structures at E||a polarization and J_{ph}^b at E||B polarization (EMF has opposite direction); C – orientation of the crystal's axes in the design of photodiodes with two pn-junctions

the nature of the spectral dependence of J_{ph} near λ₀ (654nm). The wave vector K is perpendicular to the C axis in these measurements, however, the partial effect of gyrotropy occurs because light rays are focused on the surface of the photodetector, and thus, some of them are oriented at an angle to the C axis.

The absorption coefficient is lower at E||c, E⊥B light polarization, that it is at E||B, E⊥c polarization in the shorter wavelengths' part of λ₀ (654nm). The lightwaves penetrate to the active region of photodiode 2 and give a conditionally positive sign of photo-voltage. The lightwaves are mostly absorbed in the active region of the diode 1 at E||B, E⊥c polarizations creating an inverse photo-voltage^[2, 6, 18]. The spectral characteristics of the device can be varied by changing the polarization of lightwaves incident on the surface of the coupled photodiode.

Figure 10, A shows the transmittance spectra T* of CdP₂ crystals doped with sulfur placed between crossed polarizers. The transmittance spectra are almost identical with those for undoped crystals. There is a slight difference in the λ > 750nm region. These data suggest that gyrotropy properties represent natural but not the one induced by the impurity states. The transmittance spectra of doped crystals are higher at E||B (T_b) polarization than those at E||a (T_a) polarization, in the λ > 654nm (λ > λ₀) region, Figure 10, B. The lightwaves penetrate shallower at E||a polarization, i.e. create a photo-voltage J_{ph}^a in the active region 1 (conventionally, has a positive direction). The waves' polarization corresponds to E||B case if turning the polarization plane of the incident waves by 90°. The transmittance coefficient T_b is higher at this polarization than in E||a case. The waves penetrate

Full Paper

the spatial charge region of the diode 2 (Figure 10, C) creating a photo-EMF in this area. If the thickness of the crystal is corresponding and provides a plane rotation of polarized of lightwaves up to 90°, the photo-voltage will fit to polarized waves at E||B. The J_{ph}^b photo-voltage has opposite direction to J_{ph}^a photocurrent (conventionally negative).

CONCLUSIONS

The spectral dependences of the refractive indices n_o, n_e determined from the interference transmittance spectra between crossed polarizers and form reflection spectra using the Kramers-Kronig method intersect at λ_o wavelength in CdP₂ crystals. The crystals are isotropic at λ_o wavelength and there is a maximum transmittance between crossed polarizers and Δn=n_o-n_e=0. In the long wavelength region of λ_o the value of the refractive index n^{k||c} is higher than that at n^{k||y} polarization; the dispersion is positive. In the short wavelength region there is an inverse relationship, the dispersion is negative.

Such crystal represent itself a phase plate, in which two light waves propagate with the speed V_x=c/n^{k||c} and V_y=c/n^{k||y}. The current-voltage characteristics of Ni-CdP₂ diodes had been researched at different temperatures, the temperature dependence of the “imperfection” coefficient δ for different Schottky barriers was, also, studied. The voltage – capacity characteristics of Me-CdP₂ photodiodes obtained by the electrochemical deposition of metal and thermo-chemical metal spray in vacuum on the surface of CdP₂ crystals was considered. The dependence of diffusion potential Φ_B on the metal work ξ_m(C) was estimated. The birefringence and gyration phenomenon affect the spectral characteristics of p-n photodiodes and Schottky diodes. The possibility of gaining control over the characteristics of photodiodes using the features of gyration in CdP₂ crystals was achieved.

REFERENCES

[1] V.B.Lazarev, V.J.Sevcenco, J.H.Grinberg, V.V.Sobolev; ‘Semiconductors compounds A^{II}B^V’, Nauca; Moscow, [in Russian], (1978).
 [2] N.N.Syrbu; ‘Optoelectronic properties of II–V com-

pounds’, Kishinev, [in Russian], (1983).
 [3] N.N.Syrbu, I.G.Stamov, A.I.Kamertsel; Phys.and Tech.of Semiconductors, **26(7)**, 1191 (1992).
 [4] R.Bindemann, H.Fisher, K.Kreher, N.N.Syrbu; Phys.St.Sol.(b), **69(2)**, K79 (1975).
 [5] N.N.Syrbu, I.G.Stamov; Semiconductors, **25(12)**, 2115 (1991).
 [6] N.N.Syrbu, I.G.Stamov, V.I.Morozov, V.K.Kiossev, L.G.Peev; Proc.I Int.Symp.Phys.Chem.II-V Comp.Mogilany.Poland, 237 (1980).
 [7] I.G.Stamov, D.V.Tkacenco; Semiconductors, **42(9)**, 1079 (2008).
 [8] I.G.Stamov, D.V.Tkacenco; Semiconductors, **40(10)**, 1196 (2006).
 [9] N.Sobotta, H.Neumann, V.Riede, N.Syrbu; Solid State Communications, **48(3)**, 297 (1983).
 [10] N.N.Syrbu, V.E.Livin; Semiconductors, **25(10)**, 1765 (1991).
 [11] N.N.Syrbu, V.E.Livin; Semiconductors, **25(2)**, 238 (1991).
 [12] N.N.Syrbu, V.E.Livin; Semiconductors, **24(11)**, 1911 (1990).
 [13] V.M.Trukhan, A.U.Sheleg, I.F.Fekeshgazi; Photoelectronics, **13**, 200 (2004).
 [14] V.A.Zuev, V.G.Fedotov, A.G.Bickov, E.M.Smolearenko, V.M.Truhan, V.N.Iakimovic; Soviet Journal of Quantum Electronics, **34**, 57 (1988).
 [15] V.M.Truhan, A.U.Sheleg, and all; Patent Belorus №12388, (30.10.2009).
 [16] V.V.Borsc, M.P.Lisica, P.E.Vozoli, I.V.Fecesgazi; Soviet Journal of Quantum Electronics, **22**, 41 (1982).
 [17] A.U.Sheleg, A.A.Kutas, V.N.Iakimovic, V.G.Fedotov, D.N.Karlikov, L.M.Gorynia; Patent SU, № 875959, (22.06.1981).
 [18] N.N.Syrbu, I.G.Stamov, A.G.Umanetc; Patent SU, 1865040, (14.05.1981).
 [19] N.N.Syrbu, S.I.Radautsan, I.G.Stamov, G.A.Kudinceva, A.Ju.Kasmertsel; Patent SU, № 950080, (07.04.1982).
 [20] N.N.Syrbu, I.G.Stamov, A.G.Umanetc; Patent SU, № 816345, (21.11.1980).
 [21] A.A.Andreev, B.T.Meleh, V.M.Truhan; Patent SU, № 621254, (27.04.1978).
 [22] N.N.Syrbu, I.G.Stamov, A.G.Umanetc, L.F.Buga; Patent SU, № 776440, (07.07.1980).
 [23] I.G.Stamov, N.N.Syrbu, V.K.Kiosev; Patent SU, № 824835, (22.12.1980).
 [24] V.P.Novikov, A.U.Sheleg, V.M.Truhan, V.G.Fedotov, A.G.Byckov, D.N.Karlikov, L.M.Gorynea; Patent SU, № 917004, (01.12.1981).